Received: 12 July 2020 | Revised: 8 December 2020 | Accepted: 7 January 2021

DOI: 10.1002/2050-7038.12807

RESEARCH ARTICLE

WILEY

A new transform discrete wavelet technique based on artificial neural network for induction motor broken rotor bar faults diagnosis

Mabrouk Defdaf[1,2] | **Fouad Berrabah**[1,2] | **Ali Chebabhi**[1] | **Bilal Djamal Eddine Cherif**[1]

[1]Department of Electrical Engineering, Faculty of Technology, University of M'sila, M'sila, Algeria

[2]LSELM Laboratory, Badji Mokhtar Annaba University, Annaba, Algeria

Correspondence
Mabrouk Defdaf, Department of Electrical Engineering, Faculty of Technology, University of M'sila, M'sila 28000, Algeria

LSELM Laboratory, Badji Mokhtar Annaba University, Annaba, 23000, Algeria.
Email: mabrouk.defdaf@univ-msila.dz

Summary

The main objective of this article is to contribute the automatic fault diagnosis of broken rotor bars in three-phase squirrel-cage induction motor using vibration analysis. In fact, two approaches are combined to do so, based on signal processing technique and artificial intelligence technique. The first technique is based on discrete wavelet transform (*DWT*) to detect the harmonics that characterize this fault, using the Daubechies wavelet vibration analysis according to three axes (*X*, *Y*, *Z*). This application permits having the approximation mode function and the details (*recd*). To exact choice of reconstruction details which contains the information of the broken rotor bars faults, two statistical studies based on the root mean square values (*RMS*) and Kurtosis shock factor calculation are carried out for each (*recd*). The choice of (*recd*) is conditioned by (*RMS*) and Kurtosis values as: $RMS_{recd1} < RMS_{recd2}$ and $Kurtosis_{recd1} > Kurtosis_{recd2}$. Experimental results showed that ($recd_1$ and $recd_2$) satisfied the condition set for (*RMS*) and Kurtosis values. At the end of first technique, a spectral envelop of $recd_1$ is adopted to detect the broken rotor bars fault and the second technique based on artificial neural network (*ANN*) is used to identify the number of broken rotor bars. The characteristics of features used as input variables of ANN are the RMS of $recd_1$ and $recd_2$, and the Kurtosis shock factor of $recd_1$ and $recd_2$. The experimental results demonstrated the high efficiency of the proposed method with rotor broken bars fault classification rate of 98.66%.

KEYWORDS

ANN, BRB, DWT, IM, spectral envelope, vibration analysis

List of Symbols and Abbreviations: *A*, approximations; a_0, dilation parameter; *ANN*, artificial neural network; *ANFIS*, adaptive neural fuzzy inference system; b_0, translation parameter; *CWT*, continuous wavelet transform; *D*, details; *db*, shapes of Daubechies wavelets; *DWT*, discrete wavelet transform; *f*, viscous coefficient of friction; f_b, frequency of broken rotor bar fault; f_g, sliding frequency; f_p, frequency of poles; f_r, frequency of rotation; f_s, fundamental frequency of network; f_{vb}, frequency of broken rotor bar fault with vibration analysis; F_e, sampling frequency; g, sliding; *IM*, induction motor; *J*, moment of inertia; *K*, Kurtosis shock factor; L_s and L_r, stator and rotor inductance, respectively; $M_{s,r}$, mutual stator–rotor inductance; *MMF*, magneto-motive force; *n*, number of decomposition of vibration signals; *p*, number of poles; R_s and R_r, stator and rotor resistance, respectively; *Recd*, approximation mode function and the details; *RMS*, root mean square values; *STFT*, short-time Fourier transform; t_{acq}, acquisition time; T_{em}, electromagnetic torque; T_r, resistant torque (load); *WT*, wavelet transform; *X*, *Y*, *Z*, axes of measures; θ_r, angle of displacement; ω_r, rotation speed.

1 | INTRODUCTION

The induction machine has long been strongly challenged to the synchronous machine in the fields of high power, until the advent of power electronics. The greatest use of this machine is due to standardization, its great robustness, and its low cost of purchase and maintenance.[1] The history of fault diagnosis and protection goes back to the origin of machines themselves.

The manufacturers and users of electrical machines initially implemented simple protection such as over current, overvoltage, and earth fault protection for ensure safe and reliable operation. As the tasks performed by these machines became more and more complex, improvements were also sought in the field of induction machine fault diagnosis. The diagnose faults from their birth (incipient faults) in certain applications, it has now become very important, because a failure in one of the machine component parts can paralyze the entire production process, which causes heavy financial losses.[2,3]

In the electromechanical systems diagnosis, we are essentially two parts: the first is electrical engineers for currents and voltages measurement, and the second is mechanical engineers for vibrations measurement.[4]

The diagnosing faults methods are very varied. They are distinguished based on their type of knowledge used to check the consistency between real and reference observations. Among these methods, a method based on the signal approach and calls upon signal processing techniques (Spectral analysis, Fourier transforms on a Sliding Window and transformed into Wavelets).[5,6] The wavelet transform (*WT*) method appeared in early 1990s, it affects many areas of mathematics, including signal and image processing, and is a new tool particularly suitable for the analysis of non-stationary vibration signals.

Unlike the short-time Fourier transform (*STFT*) where the window size is fixed for the entire signal analysis.[7,8] The wavelet transform uses sizes of variable window (the mother wavelet) for the entire signal, which provides good resolution in term of time and frequency. Its principle is based on the decomposition of a signal into wavelet coefficients of different scales in the time domain.

There are several types of mother wavelets, which can be used to detect and diagnose faults in rotating machines such as: Haar, Meyer, Daubechies, Morlet, etc. Therefore, WT gives good results if the mother wavelet is carefully selected.[9]

Over the past two decades, numerous studies have focused on broken rotor bars faults detection and analysis. References 10 and 11 present the *WT* role for stator current signals of an induction motor analysis with squirrel cage linked of broken rotor bars faults in starting or transient regime. In Reference 12, the *WT* is used to detect broken rotor bars and short-circuit ring portions based on fact that any failure at the rotor, this is induces a deformation in air gap magneto-motive force (*MMF*) which results in additional components in the stator currents. The authors[13] then proposed to use the STFT to detect and locate the broken rotor bar fault. The spectrogram is evaluated and used for stator currents analysis in presence of broken bar fault. In Reference 14, a study based on continuous wavelet transform (*CWT*) with multilevel decomposition of stator currents signals for detected and located the broken bars faults. The work of Mohamed et al.[15] demonstrated the good performances of discrete wavelet transform (*DWT*)-based adaptive neural fuzzy inference system (*ANFIS*) approach in terms of stator currents signals analysis for induction motor with broken rotor bars faults. The major problem of these approach based fuzzy logic is the calculation time of the identification algorithm, which is always longer. It is therefore interesting to use learning techniques to automate the fuzzy logic focus for fault detection and localization. Taking into account the properties of artificial neural networks (ANNs) in terms of computation and learning speed. In this work, we will use the ANNs in fault detection and localization of broken rotor bars in three-phase squirrel-cage induction motor.

Firstly, the paper presents a detailed mathematical modeling of an induction multiples windings motor. The technique based on *DWT* for detect the broken rotor bars faults based on harmonics characteristic by using the vibration signal decomposition based on "*Daubechies 27*" mother wavelet is then proposed. The ANN is finally used to locate the number of broken rotor bars faults.

2 | DETECTION OF INDUCTION MOTOR BROKEN ROTOR BARS

Well-known approaches for detecting broken rotor bar faults are based on the spectral analysis of stator currents to detect harmonics around the fundamental as well as other space harmonics, and the measurements of the harmonics of several measurable quantities, such as the motor torque, the speed, and the axial flow and the vibration are also used to determine the rotor faults nature[16]:

- **Stator current analysis:**

$$f_b = f_s(1 \pm 2g) \tag{1}$$

- **Mechanical torque analysis:**

$$f_b = f_s\left[\frac{N_r(1-g)}{p} \pm n\right] \pm 2g \tag{2}$$

- **Vibration analysis:**

$$f_{bv} = f_r \pm f_p \tag{3}$$

3 | SQUIRREL-CAGE INDUCTION MOTOR MODEL

In our study, the model of induction motor is introduced with symmetrical constitutions of stator is considered to allow having a sinusoidal MMF in the air gap and rotor is considered as a set of meshes, interconnected between them, each formed by two adjacent bars, connected by two portions of rings Figure 1. This model makes it possible to study the influence of a broken rotor bars faults on the general behavior of induction motor.[17,18]

The three phase's stator and rotor voltages are then written[19,20]:

$$\begin{cases} [U_s] = [R_s][I_s] + \dfrac{d[\psi_s]}{dt} \\ [U_r] = [R_r][I_r] + \dfrac{d[\psi_r]}{dt} \end{cases} \tag{4}$$

The stator and rotor flux matrix are given by:

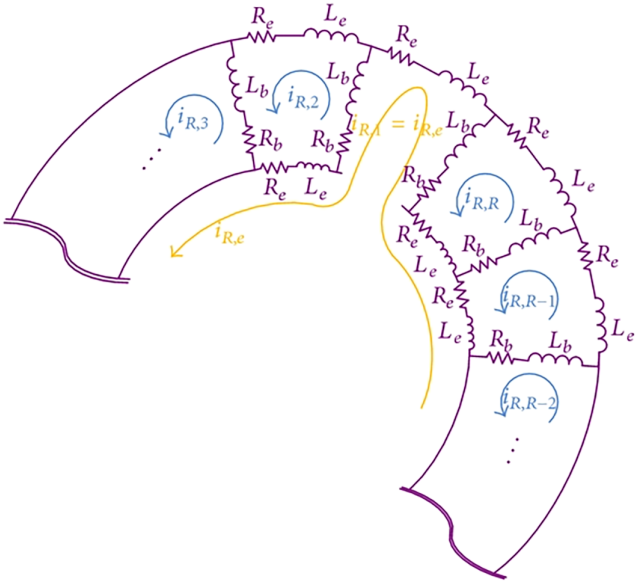

FIGURE 1 Squirrel cage IM equivalent circuit

$$\begin{cases} [\psi_s] = [L_{ss}][I_s] + [M_{sr}][I_r] \\ [\psi_r] = [L_{rr}][I_r] + [M_{rs}][I_s] \end{cases} \tag{5}$$

With $[U_s]$, $[I_s]$, and$[\psi_s]$ are the matrix of stator voltages, stator currents, and stator flux, respectively; $[U_r]$, $[I_r]$, and $[\psi_r]$ are the matrix of rotor voltages, rotor currents, and rotor flux, respectively; $[R_s]$ and $[R_r]$ are the matrix of stator resistance and rotor resistance, respectively; $[L_{ss}]$ and $[L_{rr}]$ are the matrix of stator inductance and rotor inductance, respectively; and $[M_{sr}]$ is the mutual matrix stator–rotor.

The mechanical equations are gives as:

$$J\frac{d\omega_r}{dt} = T_{em} - T_r - f\omega_r$$

$$\omega_r = \frac{d\theta_r}{dt} \tag{6}$$

$$T_{em} = \frac{1}{2}\begin{bmatrix}[I_s]\\[I_r]\end{bmatrix}^T \frac{d}{d\theta}\begin{bmatrix}[L_s] & [M_{sr}]\\[M_{sr}] & [L_r]\end{bmatrix}\begin{bmatrix}[I_s]\\[I_r]\end{bmatrix} \tag{7}$$

where T_{em} is the electromagnetic torque; T_r is the resistant torque (load); J is the moment of inertia; f is the viscous coefficient of friction; θ_r is the angle of displacement; and ω_r is the rotation speed.

4 | PRESENTATION OF THE TEST RIG

The main experimental tests that we present in this article are performed in our laboratory. According to the element affected (broken rotor bars: 1, 2, and 4 bars) each fault has a characteristic frequency which is reflected in the vibratory signal at specific frequencies well determined. The motor used in the experimental tests for the study of rotor bars breaking faults is a three-phase induction motor of AZAZGA type, delta coupling, 50 Hz, 4 poles, 3 Kw, with several rotors of the same type that can be loaded according to the broken bars number. Each of them is a single squirrel cage with 28 bar inclined bars and the stator current I is the 7 A, this last supplied by a three-phase two-level voltage inverter controlled by the via space vector pulse width modulation technique using a 1104 DSPACE card coupled to a 2.4 Kw direct current generator forming the test rig.

The measurement chain includes three Hall Effect current sensors FLUCK i30s type (AC/DC CURRENT CLAMP), three sensors voltage TEKTRONIX P5200 type, one vibration sensor type, and acquisition board (NATIONAL INSTRUMENT BNC-2110) type.

The assembly system is connected to a PC computer for viewing and processing the sensed signals. The acquisitions were performed in permanent regime with a sampling frequency equal to $F_e = 5000\ Hz$ and an acquisition time equal to $t_{acq} = 20\ s$ and the frequency resolution equal to $\Delta f = 0.05Hz$.

Figure 2 shows the vibration signals of experimental set up inverter-induction motor for different operating mode cases (normal operating case [no fault condition], 1 BRB, 2 BRB, and 4 BRB).

The flow chart of proposed technique for squirrel cage broken bars rotor fault detection is represented by the flowchart in Figure 3 as follows.

5 | DISCRETE WAVELETS TRANSFORM

A wavelet is an elementary function, with real or complex values, highly concentrated both in time and frequency. It must meet two criteria[21]:

- It must have a compact support, that is, it is localized over a small period of time,
- It must be of average zero.

FIGURE 2

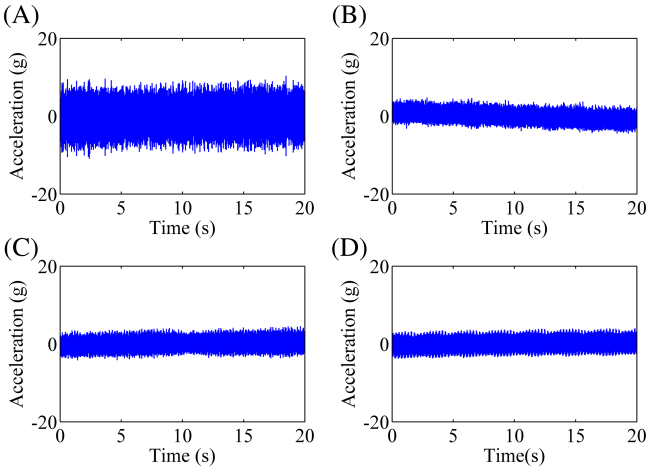

FIGURE 3

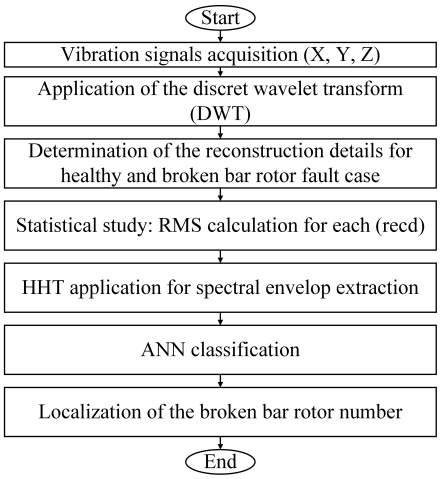

$$\int_{-\infty}^{+\infty} \psi(t)dt = 0 \tag{8}$$

It is the condition of admissibility which gave the name of wavelet. The wavelet transform of a signal $y(t)$ is defined by the formula[22]:

$$C_{a,b} = \int_{-\infty}^{+\infty} y(t).\psi_{a,b}(t)dt \tag{9}$$

The wavelet transform of a signal $y(t)$ is the family $C_{(a,b)}$ of wavelet coefficients which depends on two parameters a and b, these parameters can be used continuously (*CWT*) or discrete (*DWT*).

From the mother wavelet $\Psi(t)$, a family of functions $\Psi_{a,\,b}(t)$; which are its basic atoms; is constructed by translation and expansion. These functions of $\Psi_{a,\,b}(t)$ are given by the following relation[7]:

$$\psi_{a,b} = \frac{1}{\sqrt{a}}\psi\left(\frac{t-b}{a}\right) \tag{10}$$

The parameter b represents its time axis translation; on other hand, the parameter a gives the frequency of wavelet control; knowing that $a = \frac{1}{f}$.

- If $a < 1$, the wavelet $\Psi_{a,\,b}(t)$ becomes very concentrated compared to the mother wavelet $\Psi(t)$ and its frequency content will tilt toward the high frequencies of the analysis plane.
- If $a > 1$, the wavelet $\Psi_{a,\,b}(t)$ is very wide and the frequency content will tilt toward the low frequencies of the analysis plane.

The DWT uses a discretized scale factor and translation. In this case the parameters a and b become:

$$a = a_0^m \quad et\ b\ =\ nb_0a_0^m \qquad n,m \in Z$$

With a_0 is a dilation parameter and b_0 is a translation parameter.

Any wavelet base working with a scaling factor is called a *DWT*. This type of transform is practical in implementation on any digital system.[23]

5.1 | Daubechies wavelets

This family of wavelets has a parameter allowing manipulating orthogonal wavelets with compact support of arbitrary regularity. For N, it is the order of wavelet db_N.[24] For $N = 1$, the wavelet is db_1 and it is only the Haar wavelet. Figure 4 shows the shapes of Daubechies wavelets for different orders.

This wavelet family has the following properties:

- The wavelets db_N are asymmetrical, in particular for low values of N, except for the Haar wavelet,
- The regularity increases with the order N,
- The analysis is orthogonal.

5.2 | Multi-resolution

This technique consists a decomposing the signal with wavelet transform through two filters. One is a low pass to get the approximations that represent the general form of signal, and the other is a high pass to get its details. The approximations and details are expressed by the following two equations[25]:

$$A_{j,k} = \sqrt{2}\sum_{-\infty}^{+\infty} h[n]A_{j-1,2k+n} \tag{11}$$

$$D_{j,k} = \sqrt{2}\sum_{n=-\infty}^{+\infty} g[n]A_{j-1,2k+n} \tag{12}$$

Figure 5 shows the general form of signal during decomposition.

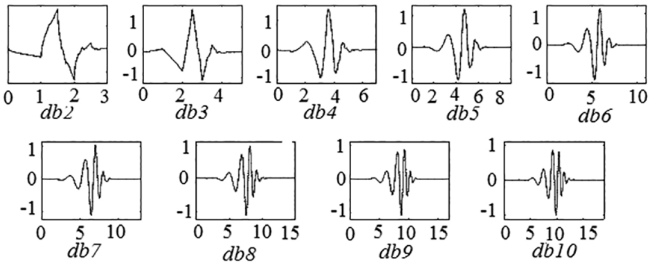

FIGURE 4 Shape of Daubechies wavelets

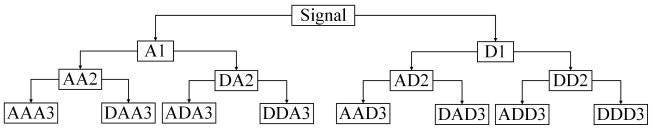

FIGURE 5 Signal decomposition into approximations and details

The decomposed signal is therefore written in the following form:

$$y(t) = D_1(t) + D_2(t) + D_3(t) + A_3(t) \tag{13}$$

For each diagnostic approaches based on the wavelet decomposition, the number of levels must be chosen judiciously in order to allow the high level signals (approximation and details) to cover the whole range of frequencies along which the component due to the faults changes during all operating modes. The number of decomposition of vibration signals are given by the following relation[26]:

$$n = 2\log\left(\frac{F_e}{4}\right) \tag{14}$$

With F_e is the sampling frequency.

Figure 6 shows the reconstructions details 1 and 2 of vibration signal from both IM healthy case and with IM faulty case: 1, 2, and 4 bars faults.

6 | STATISTIC STUDY

Two scalar indicators are used:

RMS value: This is a very characteristic value of the signal, since it has a direct relationship with the energy contained in it[27]:

$$RMS = \sqrt{\frac{1}{T}\int_t^t recd_n(t)dt} \tag{15}$$

Kurtosis (K): Mathematically, it is the moment of order 4, which is commonly, called "Kurtosis" in signal processing. It represents the flattening rate of the distribution and gives an evaluation of the importance of the peak of the top of the curve. It is defined by[28]:

$$K = \frac{1}{N}\sum_{i=1}^{N}\left|\frac{recd_n - \bar{recd_n}}{\sigma}\right|^4 \tag{16}$$

Table 1 summarizes the values of RMS and Kurtosis.

According to the criteria of kurtosis and *RMS*. It can be observed that the two details $recd_1$ and $recd_2$ satisfy the conditions: $RMS_{recd1} < RMS_{recd2}$ and $Kurtosis_{recd1} > Kurtosis_{recd2}$.

The analytical signal $\hat{recd_1}(t)$ of the signal $recd_1(t)$ can be constituted by $recd_1(t)$ and it is $HT\left(\hat{recd_1}(t)\right)$:

$$\bar{recd_1}(t) = recd_1(t) + j\bar{recd_1}(t) \tag{17}$$

The process can be followed by taking the absolute value of the analytical signal to generate the envelope[29]:

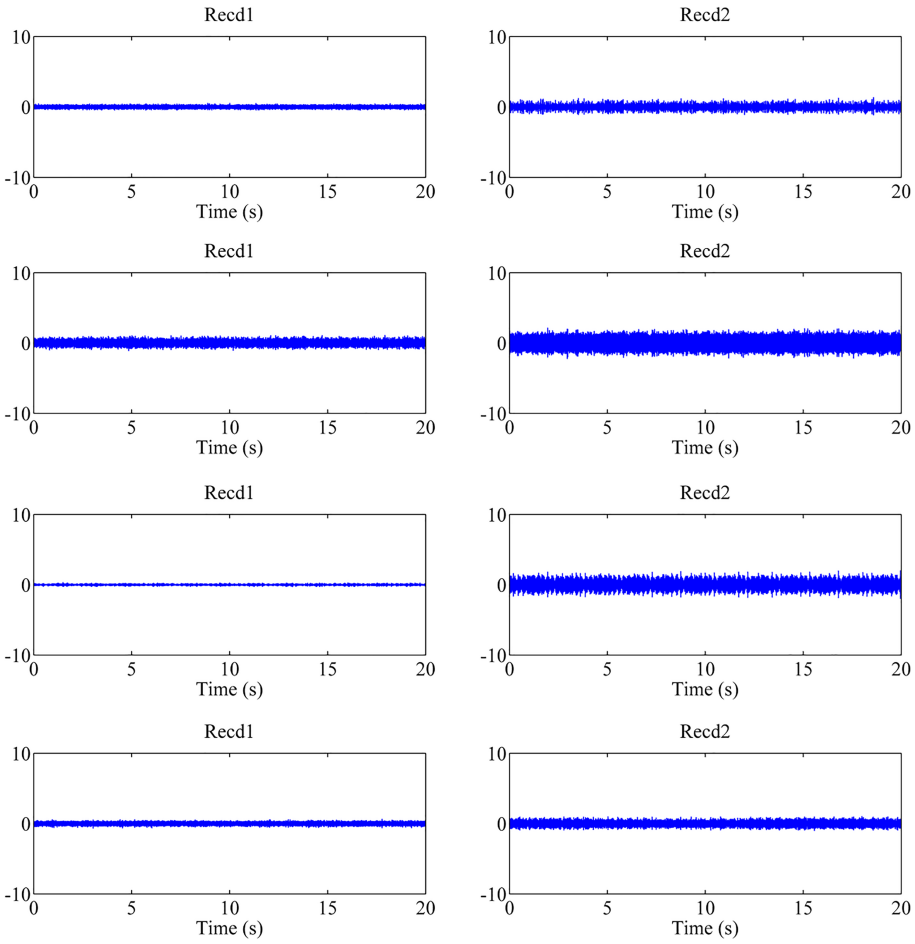

FIGURE 6

$$\left|\overline{recd}_1(t)\right| = \sqrt{recd_1(t)^2 + \overline{recd}_1(t)^2} \tag{18}$$

Figure 7 shows the spectrum of $recd_1$ for the healthy case and faulty case 1 BRB, 2 BRB, and 4 BRB.

7 | CALCULATION OF THE BROKEN ROTOR BAR FAULT FREQUENCIES

The rotation frequency is given by:

$$f_r = \frac{n}{60} \tag{19}$$

The poles frequency is given by:

$$f_p = p \times f_g \tag{20}$$

where p is the number of poles.

TABLE 1 RMS and K values

	Details						
	Healthy state						
Indicators	**Recd$_1$**	**Recd$_2$**	**Recd$_3$**	**Recd$_4$**	**Recd$_5$**	**Recd$_6$**	**Recd$_7$**
RMS value	0.1218	0.2146	2.0942	1.6288	0.0342	0.1174	0.0961
Kurtosis (K)	3.1557	2.1261	3.2720	2.8439	3.1562	2.1860	1.6126
1BRB							
RMS value	0.1969	0.5275	0.9658	0.5874	0.0334	0.0586	0.0494
Kurtosis (K)	4.2641	2.8460	2.9452	2.5082	2.9699	1.7725	1.5692
2BRB							
RMS value	0.1331	0.2042	0.6415	0.5295	0.0372	0.0677	0.0990
Kurtosis (K)	3.2069	3.0336	2.8700	2.3914	1.7111	2.6956	1.5372
4BRB							
RMS value	0.0588	0.4258	1.0161	0.6026	0.0241	0.0218	0.0795
Kurtosis (K)	4.1567	3.1656	2.7571	2.5958	3.2887	2.8406	1.5265

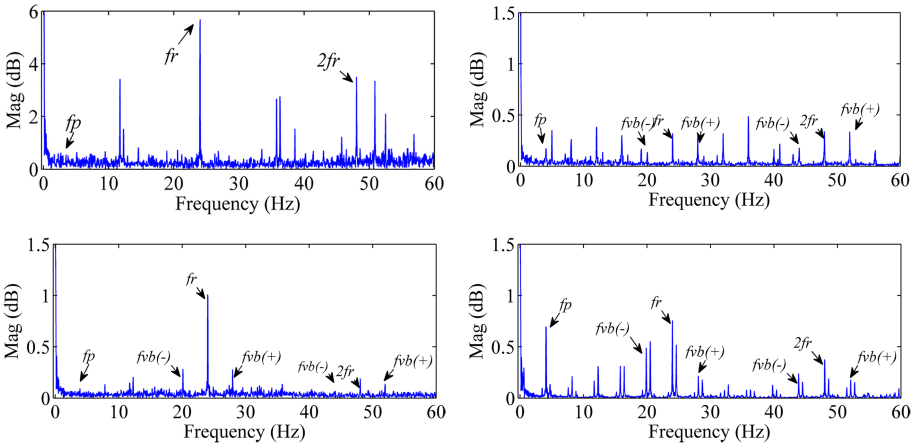

FIGURE 7

The slip frequency is given by:

$$f_g = 2 \times \frac{f_s}{p} - f_r \tag{21}$$

The broken rotor bar fault frequency is given by:

$$f_{vb} = n \times f_r \pm f_p \tag{22}$$

n : 1, 2, 3, 4...

The spectrum analysis of the healthy case shows no fault signature around 23.99 Hz (f_r). However, in the presence of a broken fault: 01, 02, and 04 bars. Two harmonics appear at: 19.99 and 28.05 Hz with the presence of the 4.082 Hz harmonic (f_p).

Table 2 summarizes the harmonics values characterizing the faults.

The values, reported in Table 3, clearly show an increase in amplitudes at specific frequencies in the case of a break of 1 BRB, 2 BRB, and 4 BRB. This table enables us to demonstrate the severity of the fault.

TABLE 2 Harmonics values of spectrum $recd_1$

		f_p	$f_{vb(-)}$	f_r	$f_{vb(+)}$	$f_{vb(-)}$	$2f_r$	$f_{vb(+)}$
Theoretical results		4 Hz	20 Hz	24 Hz	28 Hz	44 Hz	48 Hz	52 Hz
Experimental Results		4.082 Hz	19.99 Hz	23.99 Hz	28.05 Hz	43.96 Hz	47.99 Hz	52.05 Hz
	Healthy	0	0	5.678 dB	0	0	3.502 dB	0
	01 BRB	0.053 dB	0.181 dB	0.818 dB	0.191 dB	0.071 dB	0.118 dB	0.090 dB
	02 BRB	0.303 dB	0.243 dB	1.268 dB	0.251 dB	0.288 dB	0.833 dB	0.168 dB
	04 BRB	0.813 dB	0.521 dB	0.723 dB	0.264 dB	0.362 dB	0.457 dB	0.194 dB

TABLE 3 Characteristics of proposed artificial neural network

Number of input nodes	**04**	**02 *RMS* nodes of $recd_1$ et $recd_2$** **02 *Kurtosis* nodes of $recd_1$ et $recd_2$**
Number of output nodes	03	Desired output = [YXX] Y = 0 : For healthy state. Y = 1 : For Fault ydr CWgg& state. X = 00 : For healthy state; 01 : broken fault case 01 bar; 10 : broken fault case 02 bars; 11 : broken fault case 04 bars.
Number of hidden layers	03	Layer 01 : 21 nuerons Layer 02 : 14 nuerons Layer03 : 07 nuerons

8 | ARTIFICIAL NEURAL NETWORK APPLICATION FOR LOCATING THE NUMBER OF BROKEN BARS

The ANN used in our work consists of 05 layers, an input layer, three hidden layers and an output layer. The characteristics representative of the healthy and faulty states used for learning and testing correspond to:

- RMS value of detail reconstruction 01;
- Kurtosis values of detail reconstruction 01;
- RMS value of detail reconstruction 02;
- Kurtosis values of detail reconstruction 02.

The final structure is chosen according to the error minimization between the real and desired value. The ANN model obtained is composed of the optimal weight and the vector of bias. The neural network structure selected is presented in Table 3.

The learning process will stop when one of these following conditions is met:

- The maximum number of iterations (epochs) = 300 000;
- The mean square error = 0.0001.
- The performance gradient $\leq 1 \times 10^{-6}$

Figure 8 shows the proposed ANN model and the learning performance.

To evaluate the classification performance, two different data sets are collected from both the healthy and faulty case. Table 4 illustrates the results obtained from optimal structure when taking into account the desired output. The actual classification rate of our diagnostic system is 98.66% (see Table 4) which demonstrates the efficiency of the architecture. Several tests are performed to obtain the optimal structure and results.

The values obtained indicate that the ANN model classification chosen has experienced considerable success in the detection and classification of broken rotor bar faults.

FIGURE 8

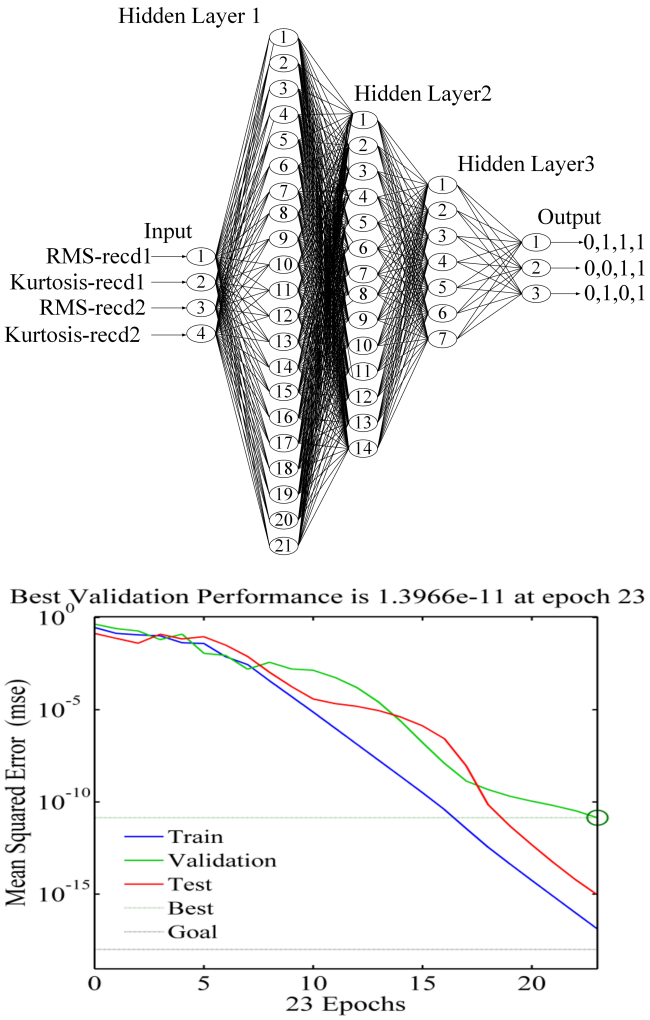

TABLE 4 Performance of selected artificial neural network

State	Desired output	Real output	Classification rate
Healthy state	0 0 0	0.0098 0.0098 0.00098	98.66%
Faulty state 01 broken bar	1 0 1	0.9998 0.0098 0.9998	
Faulty state 02 broken bar	1 1 0	0.9998 0.9998 0.0098	
Faulty state 04 broken bar	1 1 1	0.9998 0.9998 0.9998	

9 | CONCLUSION

In this paper, the diagnosis of an induction motor broken rotor bar fault based on vibration analysis technical by using the combined discrete wavelet transform and ANN is proposed. The experimental study focuses on a two-level three-phase voltage inverter fed induction motor controlled by an space vector pulse width modulation technique. The experimental approach makes it possible to validate the theoretical frequencies characterizing the broken rotor bar faults. The results obtained by the combined discrete wavelet transform and ANN technique used for the various broken rotor bars faults (01 BRB, 02 BRB, and 04 BRB), have shown that the proposed new technical studied are complementary. Indeed, the proposed new technical cannot only detect the broken rotor bar fault but can also locate easily the number of broken rotor bars. However, it is found that the type of power supply used conditions the reliability of the proposed technique used. Indeed, the use of an inverter makes the vibration spectrum richer in harmonics.

PEER REVIEW

The peer review history for this article is available at https://publons.com/publon/10.1002/2050-7038.12807.

DATA AVAILABILITY STATEMENT

Research data are not shared.

ORCID

Mabrouk Defdaf https://orcid.org/0000-0002-9100-057X
Bilal Djamal Eddine Cherif https://orcid.org/0000-0001-7703-2295

REFERENCES

1. Thakur A, Wadhwani S, Wadhwani AK. Motor current signature analysis as a tool for induction machine fault diagnosis. *Int J Comput Sci Inf Technol Res*. 2015;3(3):309–313.
2. Foued L. Surveillance des machines par analyse vibratoire. Support de cours. www.coursehero.com.
3. Taylor JI. *The Vibration Analysis Handbook. Livre*. 1st ed. Lebanon, OH: Edition Vibration Consultants; 2003.
4. Delgado-Arredondo PA. *Methodology for Fault Detection in Induction Motors via Sound and Vibration Signals*. Cambridge, MA: Science Direct/Elsevier; 2017.
5. Ouanas A, Medoued A, Haddad S, Mordjaoui M, Sayad D. Automatic and online detection of rotor fault state. *Int J Renewable Energy Dev (IJRED)*. 2018;7(1):43-52. https://doi.org/10.14710/ijred.7.1.43-52.
6. Medoued A, Lebaroud A, Laifa A, Sayad D. Classification of induction machine faults using time frequency representation and particle swarm optimization. *J Electr Eng Technol*. 2014;9(1):170-177. https://doi.org/10.5370/JEET.2014.1.170.
7. Keskes H, Braham A, Lachiri Z. Broken rotor bar diagnosis in induction machines through stationary wavelet packet transform and multiclass wavelet SVM. *Electr Power Syst Res*. 2013;97:151-157.
8. Yan R, Gao RX, Chen X. Wavelets for fault diagnosis of rotary machines: a review with applications. *Signal Process*. 2013;96:1-15.
9. Cherif BDE, Bendiabdellah A. Detection of two-level inverter open-circuit fault using a combined DWT-NN approach. *J Control Sci Eng (JCSE)*. 2018;11. https://doi.org/10.1155/2018/1976836.
10. Anik V. Fault diagnosis of induction motor using wavelets. *Int J Res Eng*. 2017;4(4):125-126.
11. Gaeid Salloum K, Ping HW. Wavelet fault diagnosis and tolerant of induction motor: a review. *Int J Phys Sci*. 2011;6(3):358-376. https://doi.org/10.5897/IJPS10.632.
12. Bouzida A, Touhami O, Abdelli R. Application de la technique des ondelettes au diagnostic de défauts de la machine asynchrone à rotor à cage. *Rev Energ Renouv*. 2014;17(4):549-557.
13. Aimer AF, Boudinar AH, Benouzza N, Bendiabdellah A. Simulation and experimental study of induction motor broken rotor bars fault diagnosis using stator current spectrogram. Paper presented at: 2015 3rd International Conference on Control, Engineering & Information Technology (CEIT); 2015, Tlemcen. pp. 1-7. DOI: https://doi.org/10.1109/CEIT.2015.7233037.
14. Ibrahim C, Djalal EK, Salim C. Continuous wavelet technique for detection of broken Bar faults in induction machine. *J Trait Signal*. 2019;36(2):171-176.
15. Mohamed MA, Mohamed A-AA, Abdel-Nasser M, et al. Induction motor broken rotor bar faults diagnosis using ANFIS-based DWT. *Int J Model Simul*. 2020;1-14.
16. F G, Wang T, Alwodai A, et al. A new method of accurate broken rotor bar diagnosis based on modulation signal bispectrum analysis of motor current signals. *Mech Syst Signal Process*. 2014;50(51):400-413.
17. Ghorbanian V, Faiz J. A survey on time and frequency characteristics of induction motors with broken rotor bars in line-start and inverter-fed modes. *Mech Syst Signal Process*. 2015;54:427-456. https://doi.org/10.1016/j.ymssp.2014.08.022.
18. Dorjsuren Y, Tumenbayar L, Tsevegmid J. Three-axis dynamic modeling of induction motor. *Int J Math Models Methods Appl Sci*. 2015;9:527-536.
19. Boum A, Maurice NYJ, Nneme LN, et al. Fault diagnosis of an induction motor based on fuzzy logic, artificial neural network and hybrid system. *Int J Control*. 2018;8(2):42-51.
20. Dias CG, da Silva LC, Chabu IE. Fuzzy-based statistical feature extraction for detecting broken rotor bars in line-fed and inverter-fed induction motors. *Energies*. 2019;12(12):2381.
21. Mehala N, Dahiya R. Rotor faults detection in induction motor by wavelet analysis. *Int J Eng Sci Technol*. 2009;1(3):90-99.
22. Yang Q, Wang J. Multi-level wavelet shannon entropy based method for single-sensor fault location. *Entropy*. 2015;17(10):7101-7117.
23. Kumar MN, Chandra KA. Application of wavelet transforms for alternator stator fault location and protection. *J Theor Appl Inf Technol*. 2010;16(1):77-86.
24. Cherif BDE, Azzeddine B, Mokhtar B. Detection of a two-level inverter open-circuit fault using the discrete wavelet transforms technique. Paper presented at: 19th IEEE International Conference on Industrial Technology (ICIT 2018); 2018, Lyon, France. pp. 19-22.
25. Rao RM, Bopardikar AS. *Wavelet Transforms: Introduction to Theory and Applications*. Boston, MA: Addison Wesley Longman; 1998 ISBN: 0-201-63463-5.

26. Seninete S, Mimi M, Cherif BDE, Ali AO. Vibration signal analysis for bearing fault diagnostic of asynchronous motor using HT-DWT technique. Paper presented at: 2019 6th International Conference on Image and Signal Processing and their Applications (ISPA). https://doi.org/10.1109/ISPA48434.2019.8966801
27. Cherif BDE, Bendiabdellah A, Tabbakh M. Diagnosis of an inverter IGBT open-circuit fault by Hilbert-Huang transform application. *J Trait Signal*. 2019;36(02):127-132.
28. Abdelkader R, Kaddour A, Bendiabdellah A, Derouiche Z. Rolling bearing fault diagnosis based on an improved denoising method using the complete ensemble empirical mode decomposition and the optimized thresholding operation. *IEEE Sensors J*. 2018;18(17):7166-7172.
29. Cherif BDE, Bendiabdellah A, Tabbakh M. An automatic diagnosis of an inverter IGBT open-circuit fault based on HHT-ANN. *Electr Power Compon Syst*. 2020;48(6–7):589-602.

How to cite this article: Defdaf M, Berrabah F, Chebabhi A, Cherif BDE. A new transform discrete wavelet technique based on artificial neural network for induction motor broken rotor bar faults diagnosis. *Int Trans Electr Energ Syst*. 2021;31:e12807. https://doi.org/10.1002/2050-7038.12807